Some exact solutions for debris and avalanche flows

Shiva P. Pudasaini
Department of Geodynamics and Geophysics, Steinmann Institute, University of Bonn, Nussalle 8, D-53115 Bonn, Germany and School of Science, Kathmandu University, Dhulikhel, Kavre, GPO Box 6260, Kathmandu, Nepal

(Received 27 August 2009; accepted 22 February 2011; published online 8 April 2011)

Exact analytical solutions to simplified cases of nonlinear debris avalanche model equations are necessary to calibrate numerical simulations of flow depth and velocity profiles on inclined surfaces. These problem-specific solutions provide important insight into the full behavior of the system. In this paper, we present some new analytical solutions for debris and avalanche flows and then compare these solutions with experimental data to measure their performance and determine their relevance. First, by combining the mass and momentum balance equations with a Bagnold rheology, a new and special kinematic wave equation is constructed in which the flux and the wave celerity are complex nonlinear functions of the pressure gradient and the flow depth itself. The new model can explain the mechanisms of wave advection and distortion, and the quasiasymptotic front bore observed in many natural and laboratory debris and granular flows. Exact time-dependent solutions for debris flow fronts and associated velocity profiles are then constructed. We also present a novel semiexact two-dimensional plane velocity field through the flow depth. Second, starting with the force balance between gravity, the pressure gradient, and Bagnold's grain-inertia or macroviscous forces, we construct a simple and very special nonlinear ordinary differential equation to model the steady state debris front profile. An empirical pressure gradient enhancement factor is introduced to adequately stretch the flow front and properly model nonhydrostatic pressure in granular and debris avalanches. An exact solution in explicit form is constructed, and is expressed in terms of the Lambert–Euler omega function. Third, we consider rapid flows of frictional granular materials down a channel. The steady state mass and the momentum balance equations are combined together with the Coulomb friction law. The Chebyshev radicals are employed and the exact solutions are developed for the velocity profile and the debris depth. Similarly, Bagnold's fluids are also used to construct alternative exact solutions. Many interesting and important aspects of all these exact solutions, their applications to real-flow situations, and the influence of model parameters are discussed in detail. These analytical solutions, although simple, compare very well with experimental data of debris flows, granular avalanches, and the wave tips of dam break flows. A new scaling law for Bagnold's fluids is established to relate the settlement time of debris deposition. It is found analytically that the macroviscous fluid settles (comes to a standstill) considerably faster than the grain-inertia fluid, as manifested by dispersive pressure. © *2011 American Institute of Physics*. [doi:10.1063/1.3570532]

I. INTRODUCTION

The dynamics of debris flow is described in many situations with sufficient accuracy by using a single-phase continuum of a solid-fluid mixture.[1–11] However, there are also alternative two-phase models for debris flows down general and complicated topographies in Cartesian and slope fitted coordinates.[12–15] Both types of models have been successfully applied to real-flow events in laboratory and field experiments.

In single-phase debris flow models, the mixture of fluid and solid particles is considered as a continuum fluid.[16,17] The apparent debris fluid is characterized by the constitutive relationship between the operating shear stress and the strain-rate. Examples include the Newtonian fluid and non-Newtonian fluids (e.g., Bingham, Herschel–Bulkley, and dilatant fluid). The Newtonian fluid is represented by laminar flow of pure water without any solid particles. For this, the shear stress (τ) is linearly proportional to the strain-rate ($\partial\tilde{u}/\partial z$), $\tau=\mu(\partial\tilde{u}/\partial z)$, with dynamic viscosity μ. Bingham fluids deform only if the operating stress is larger than a threshold yield stress, τ_y. Above the yield stress, it deforms as a Newtonian fluid. The relation is written as $\tau=\tau_y+\mu_B(\partial\tilde{u}/\partial z)$, where μ_B is called the Bingham fluid viscosity. Furthermore, the three parameter Herschel–Bulkley fluids are described by the relation $\tau=\tau_y+K_{HB}(\partial\tilde{u}/\partial z)^n$, $n\leq 1$, where K_{HB} is the Herschel–Bulkley consistency index, which degenerates into a Bingham fluid for $n=1$. Thus, the mobility (strain-rate) in the Herschel–Bulkley fluid is increased with increasing shear stress. Water-saturated static clay is an example of such a fluid.[6] The dilatant fluid, expressed by the relation $\tau=K_D(\partial\tilde{u}/\partial z)^n$, $n>1$, behaves quite differently than the Herschel–Bulkley fluid in that its mobility is decreased with increasing shear stress. Newtonian, two or three parameter yield strength fluids and power law or dilatant fluids are commonly used rheological models while describing debris flows as a single-phase continuum.

In reality, debris flows are such complex systems that a description by any single constitutive equation is highly improbable. However, many debris flow events are well described by Bagnold-type dilatant fluid,[6,18] $\tau=K_D(\partial\tilde{u}/\partial z)^n$. If the shear and normal stresses in the mixture (suspension) vary quadratically ($n=2$) with the shear-rate, the flow is said to satisfy Bagnold's grain-inertia flow. If this relation is linear ($n=1$), then the motion is said to satisfy Bagnold's macroviscous flow. These flow laws were derived by Bagnold in 1954 with his pioneering experiments in an annular coaxial cylinder rheometer where he evaluated the effects of grain interaction in the suspension. These types of relationships have been confirmed by many subsequent shear-cell experiments for both wet and dry mixtures[19] and computer simulations.[20,21] Note, however, as suggested by Hunt *et al.*,[22] that there can be some inconsistencies and shortcomings in Bagnold's experiments and data analysis. Bagnold's rheology can be rewritten and put in the form of a Newtonian fluid $\tau=\eta(\partial\tilde{u}/\partial z)$ in which the corrected (apparent) viscosity $\eta=K_D(\partial\tilde{u}/\partial z)^{n-1}$ is now a function of the shear-rate. For $n=1$, this corresponds to Newtonian viscous fluid with $K_D=\mu$. However, for $n=2>1$ (shear thickening) the apparent viscosity increases with increasing shear-rate and one obtains the Bagnold's dilatant fluid. Similarly, for $n<1$ the apparent viscosity decreases with increasing shear-rate and one obtains the shear thinning fluid.[23] Here we are particularly interested in two cases, $n=2$ and $n=1$.

We present three different types of new exact solutions to describe debris and granular flows down inclined slopes by employing Bagnold and dry Coulomb rheologies. Both slow and rapid flows are considered and solutions are derived for either for time-dependent or steady state conditions. These solutions are valid either in the vicinity of the moving front or down the entire slope.

The first types of solutions are constructed by combining the mass and noninertial momentum equations together with Bagnold's rheology. This results in a very special kinematic wave equation in conservative form, in which the flux and the wave celerity are highly nonlinear functions of the height and the pressure gradient. This model equation is solved for triangular initial debris profile by implementing the Total Variation Diminishing-Non-Oscillatory Central (TVD-NOC) high resolution shock capturing numerical scheme.[11,24,25] The simulation demonstrates the typical dynamics of the debris flow as it advects down-slope after its release, and induces the shock structure in the front and stretching in the tail of the debris body as observed in many debris flow events.[5,12,15,26] The kinematic wave equation is employed to construct exact solutions for the debris flow fronts and velocity profile. New and mechanically important expressions are derived to establish relationships concerning the settlement time and the settlement lengths between the grain-inertia and the macroviscous fluids. These results predict that the macroviscous fluid settles much faster than its grain-inertia counterpart. Furthermore, a new semiexact solution for the plane velocity profile through depth is constructed.

A second type of solution is derived for steady state debris flow fronts, where the force balance is maintained between Bagnold's grain-inertia or macroviscous forces, gravity, and the hydraulic pressure gradient. The pressure gradient is augmented by the pressure gradient enhancement factor, which is found to be very important to adequately stretch the flow and calibrate the model solution with experimental data. The exact solution is written explicitly in terms of the well known Lambert–Euler omega function of the mathematical physics, and the down-slope channel position. The influence of the constant and the variable shear-rate at the base is analyzed in detail.

A third type of exact solution is developed for the steady state rapid flows of granular material down a slope. The flow is either governed by the Coulomb friction or by Bagnold's law for which solutions are constructed, respectively, in terms of Chebyshev radicals or in the transcendental form. It is demonstrated that the Coulomb sliding law predicts the flow dynamics much better than the Bagnold's grain-inertia law for the flow just below the uniform release of the granular material from the silo.

Intensive parameter studies are performed to investigate the behavior and the mechanisms controlling all of the new solutions. The parameters are grouped into geometric or physical parameters. It is demonstrated that the exact solutions presented here compare either very well, or excellently, with the field and laboratory data. Our solutions conform closely with the alternative model solutions presented in the literature.[6,12,13,20,21,27]

II. KINEMATIC WAVES FOR DEBRIS FLOW FRONT

A. Grain-inertia

Let x and z be the coordinates along the channel down-slope and normal to the channel basal surface, respectively; t is the time; $\tilde{u}=\tilde{u}(x,z,t)$ and $\tilde{w}=\tilde{w}(x,z,t)$ are the local down-slope and slope normal velocity components; and h is the debris depth. Assume a mild slope with inclination angle ζ with the horizontal, and a small aspect ratio H/L, where H and L are the typical debris heights normal to the bed and extent along the bed, respectively. With this assumption, the inertial contribution can be neglected.[6,27] Therefore, the momentum balance along the down-hill direction

$$\rho\left(\frac{\partial\tilde{u}}{\partial t}+\tilde{u}\frac{\partial\tilde{u}}{\partial x}+\tilde{w}\frac{\partial\tilde{u}}{\partial z}\right)=-\frac{\partial\sigma_{xx}}{\partial x}-\frac{\partial\tau_{xz}}{\partial z}+\rho g\sin\zeta, \tag{1}$$

reduces to

$$0=-\frac{\partial\sigma_{xx}}{\partial x}-\frac{\partial\tau_{xz}}{\partial z}+\rho g\sin\zeta, \tag{2}$$

where σ_{xx} and τ_{xz} are the negative Cauchy stress components (normal and shear, respectively), ρ is the material density, and g is gravity acceleration. It is further assumed that there is a balance between gravity, pressure gradient, and Bagnold's grain-inertia stress. Then, for hydrostatic condition (see Pudasaini and Hutter[11]) with $\sigma_{xx}=K\rho g\cos\zeta(h-z)$, after integrating Eq. (2) and substituting the Bagnold's inertial stress[19] $\tau_{xz}=\rho R^2 f_{gi}\tan\phi(\partial\tilde{u}/\partial z)^2$ yields

$$\rho g \cos\zeta\left(\tan\zeta - K\frac{\partial h}{\partial x}\right)(h-z) = \rho R^2 f_{gi}\tan\phi(\partial\tilde{u}/\partial z)^2, \tag{3}$$

where K is the earth pressure coefficient,[11,28] R is the particle diameter, f_{gi} is the tensor-valued function of the solid fraction (ν), ϕ is the collision angle between grains (internal friction angle in equilibrium), and $\partial\tilde{u}/\partial z$ is the shear rate.[6,9,18,19,29,30] In Eq. (3), the first and second terms on the left-hand side represent the forces due to gravity and pressure gradient along the down-hill direction, respectively, $h-z$ accounts for the depth variation of the flow, and the right-hand side represents the Bagnold's grain-inertia stress. Note that there is no direct and explicit influence of the channel slope angle on the Bagnold's rheology for debris motion. However, the effect of the slope is implicit through f_{gi} (via ν) and $\partial\tilde{u}/\partial z$. This is so, because the driving force generated by the slope leads to changes in ν and $\tilde{u}$. A detailed investigation on this is presented in Sec. II E. By applying the no-slip condition along the basal surface,[20,21] Eq. (3) can be integrated along the flow depth to obtain

$$\tilde{u} = \frac{2}{3}\Lambda^p_{gi}[h^{3/2} - (h-z)^{3/2}], \tag{4a}$$

$$\Lambda^p_{gi} = \Lambda_{gi}\sqrt{1-\varsigma\frac{\partial h}{\partial x}}, \tag{4b}$$

$$\Lambda_{gi} = \sqrt{\frac{g\sin\zeta}{R^2 f_{gi}\tan\phi}}, \tag{4c}$$

$$\varsigma = K/\tan\zeta, \tag{4d}$$

where p indicates the presence of pressure gradient. It is important to note that, in Eq. (4a), the velocity profile is influenced by the pressure gradient which, in fact, determines the shape of the velocity field through the depth. The mean surface-parallel velocity then takes the following form:

$$u = \frac{2}{5}\Lambda^p_{gi}h^{3/2}. \tag{5}$$

This means that the mean velocity is 3/5 times smaller than the free-surface velocity. Next, we consider the mass balance equation in the depth-averaged form (see, e.g., Iverson,[12] Pitman and Le,[14] Gray *et al.*,[31] and Pudasaini and Hutter[32])

$$\frac{\partial h}{\partial t} + \frac{\partial}{\partial x}(hu) = 0. \tag{6}$$

Equation (6) combined with Eq. (5) yields a kinematic wave in the conservative form, with the flux $\mathcal{F}^p_{gi} = (2/5)\Lambda^p_{gi}h^{5/2}$, and the pressure gradient and the depth dependent nonlinear variable wave speed $\mathcal{C}^p_{gi} = \partial\mathcal{F}^p_{gi}/\partial h = C^p_{gi}(\Lambda_{gi}, \varsigma; h, \partial h/\partial x) = \Lambda^p_{gi}h^{3/2}$,

$$\frac{\partial h}{\partial t} + \frac{\partial \mathcal{F}^p_{gi}}{\partial x} = 0, \tag{7a}$$

$$\frac{\partial h}{\partial t} + \mathcal{C}^p_{gi}\frac{\partial h}{\partial x} - \mathcal{D}^p_{gi}\frac{\partial^2 h}{\partial x^2} = 0, \tag{7b}$$

where $-\mathcal{D}^p_{gi}\partial^2 h/\partial x^2$, with $\mathcal{D}^p_{gi} = (\varsigma/5)[h/(1-\varsigma\partial h/\partial x)]\mathcal{C}^p_{gi}$ as the diffusion term. Note that the wave speed $\mathcal{C}^p_{gi}$ is associated with the advection of the problem. For $\mathcal{F}^p_{gi} = h^2/2$, Eq. (7) is the Burger equation describing the nonlinear wave phenomena. A special feature of Eq. (7) is that it not only includes the flow height h but also the material parameters Λ and ς, and (importantly) the hydraulic gradient $\partial h/\partial x$ in the flux and the wave celerity. In the usual treatment of the hyperbolic equations for shallow granular flows (see, e.g., Pudasaini and Hutter,[11] Pitman and Le,[14] and Gray *et al.*[31]), the wave celerities are expressed as $u \pm \sqrt{Kg\cos\zeta h}$.

One can either use the conservative form Eq. (7a) or the nonconservative form Eq. (7b). If the nonconservative form is considered, which is an advection-diffusion equation, the advective part can be treated as the wave (hyperbolic) equation and the diffusion term (parabolic part) can generally be treated as a source term, as in Pudasaini *et al.*[15] Furthermore, the scaling analysis shows that the diffusion term is one order of magnitude higher in the shallowness parameter $\varepsilon = H/L$ (i.e., $\varepsilon^{3/2}$) compared to the advective term (i.e., $\varepsilon^{1/2}$). Following the scaling analysis as in Pudasaini and Hutter,[11,32] Iverson and Denlinger,[12] Pudasaini *et al.*,[15] Savage and Hutter,[28] and Gray *et al.*,[31] the diffusion term can be neglected. Therefore, one can deal either with the conservative form or with the nonconservative form (in which the diffusion term is neglected). Our analysis in Sec. II F for the wave phenomena is based on the conservative structure Eq. (7a) and similarity solutions in this and the following sections are constructed by considering the nonconservative form Eq. (7b) in which the diffusion term is neglected.

Next, we seek an exact solution in similarity form $\eta = -x/t$. Since $dh/d\eta \neq 0$, Eq. (7) is then transformed into a first order ordinary differential equation

$$\frac{dh}{dx} = \mathcal{A} - \mathcal{B}\frac{x^2}{h^3}, \quad \mathcal{A} = 1/\varsigma, \quad \mathcal{B} = 1/(\Lambda^2_{gi}t^2\varsigma). \tag{8}$$

It is important to observe that, in Eq. (8), the pressure gradient dh/dx is explicitly given by the right-hand side that is expressed in terms of the channel down-slope distance, flow depth, and the material parameters in which time is also considered as a parameter. Note that Eq. (8) is valid for any Λ^p_{gi}. An important observation of Eq. (8) is that the pressure gradient is proportional to x^2 and inversely proportional to h^3. Although Eq. (8) appears to be simple, it does not have an exact solution due to nonhomogeneity and can only be solved numerically for given initial condition: $h_0 = h(x = x_0)$, in which $t > 0$ is considered as a parameter. However, in the limit, as $\varsigma \to 0$, the pressure gradient is ineffective and the above problem is eliminated. Then Eq. (8) becomes a pure algebraic equation that does not require any initial or boundary condition. However, mechanically, we can choose the initial conditions as: $h_0 = h(x=0) = 0$, $u_0 = u(x=0) = 0$. So, by setting $x \mapsto -x$, the exact solutions for the debris flow height and the velocity is obtained,

$$h=\left[-\frac{1}{\Lambda_{gi}}\frac{x}{t}\right]^{2/3},\quad u=-\frac{2}{5}\frac{x}{t}. \tag{9}$$

Note that the similarity solutions such as these can be constructed with standard procedure.[27] Similarity solution means that for all times, $t>0$, the qualitative behavior of the solution remains similar (unchanged). Alternatively, if the channel slope is negligible or the channel is horizontal, Eq. (8) reduces to a separable equation $dh/dx=-\mathcal{B}_0x^2/h^3$ leading to an exact solution,

$$h=\left(h_0^4-\frac{4}{3}\mathcal{B}_0x^3\right)^{1/4},\quad \mathcal{B}_0=\frac{R^2f_{gi}\tan\phi}{gKt^2}, \tag{10}$$

for which $h_0=h(x=0)=0$ serves as the initial condition for any $t>0$.

It is important to mention that the mapping $x\mapsto -x$ is chosen only for convenience so that we are always looking at the debris flow head (at $x=0$) from the downstream perspective. With this transformation, it is easier to understand and physically interpret the flow since the mass is sliding downslope. With respect to the front advancing downstream, the flow height, h, increases in the upstream direction as measured from the nose-tip. Note also that the solutions Eq. (9) are valid for negligible pressure gradient for which the flow is mainly driven by gravity, while solutions Eq. (10) are valid for negligible slope in which the flow is mainly driven by the pressure gradient. One must solve Eq. (8) for the motion in which all three forces: gravity, pressure gradient, and the grain-inertia, are important. Moreover, if the diffusion process is also important, then Eq. (7) must be solved. Equations (7) and (8) can only be solved numerically.

B. Macroviscous

Solutions similar to Eq. (9) can also be derived for Bagnold's macroviscous fluid, $\rho g\cos\zeta[\tan\zeta-K(\partial h/\partial x)](h-z)=\rho R^2f_{mv}\tan\phi(\partial\tilde{u}/\partial z)$, which reads

$$h=\left[-\frac{1}{\Lambda_{mv}}\frac{x}{t}\right]^{1/2},\quad u=-\frac{1}{3}\frac{x}{t}, \tag{11}$$

where $\Lambda_{mv}=g\sin\zeta/(R^2f_{mv}\tan\phi)$, and f_{mv} has the dimension of the shear-rate, i.e., for the macroviscous deformation the shear-stress scales with the viscosity, and $h_0=h(x=0)=0$, $u_0=u(x=0)=0$ are the initial conditions for any $t>0$.

It is mentioned that for the macroviscous fluid, the wave equation again takes the form of Eq. (7), but with a different flux and wave celerity, namely, $\mathcal{C}^p_{mv}=\Lambda^p_{mv}h^2$, $\Lambda^p_{mv}=\Lambda_{mv}[1-\mathfrak{s}(\partial h/\partial x)]$. Furthermore, dimensional analysis shows that solutions presented in this and the following sections are also valid for mild slopes with shallow curvatures.

Note that by applying Coulomb-type frictional resistance (and assuming constant velocity), Pouliquen[33,34] and others analyzed the propagation of granular fronts of smooth particles down rough and mild inclines whose angles do not vary so much from the internal friction of the material. This resulted in a steady state slow motion of particles with small flow depth and velocity typically 0.2 ms^{-1} and 0.01 m, respectively. Here we use Bagnold fluid instead of Coulomb fluid. The advantage of such a choice is discussed later.

C. Reconstruction of the velocity field through the flow depth

The velocity field through the flow depth can be reconstructed as a function of time, channel position, and the flow depth position by inserting h from Eq. (9) into Eq. (4),

$$\tilde{u}=\frac{2}{3}\left[-\frac{x}{t}-\left\{\left(-\frac{x}{t}\right)^{2/3}-\Lambda_{gi}^{2/3}z\right\}^{3/2}\right]. \tag{12}$$

Equation (12) is a semiexact solution of Bagnold's grain-inertia fluid for the velocity field but in the form of the independent variables t, x, and z and that $\tilde{u}\propto(z^{3/2},x,1/t)$, respectively. Equations analogous to Eq. (12) can also be obtained for the macroviscous fluid.

D. A new scaling law for the settlement (depositional) behavior of Bagnold's fluids

Notice that the velocity expressions in Eqs. (9) and (11) do not involve the parameters Λ_{gi} and Λ_{mv}, so the following discussion is valid. Importantly, these equations show that the settlement process (the process that brings the debris particles to rest) is 5/6 times shorter for the macroviscous fluid than for the grain-inertia fluid,

$$u_{mv}=-\frac{1}{3}\frac{x}{t}\equiv-\frac{2}{5}\frac{x}{t}=u_{gi},\quad t_{mv}=\frac{5}{6}t_{gi},\quad x_{mv}=\frac{6}{5}x_{gi}, \tag{13}$$

where the suffixes $_{mv}$ and $_{gi}$ represent the macroviscous and the grain-inertia fluids, respectively. Here, the settlement refers to the deposition or the complete cease of the fluid motion (i.e., the fluid velocity becomes zero), but it does not refer to the solid particles' settlement down (through) a viscous fluid, e.g., as in Stokes flow. We are also using this term for convenience in the context of the present paper. Hence, given the same time, the macroviscous fluid is settled 6/5 unit length compared to the unit length settlement of the grain-inertia fluid as measured from the nose-tip of the flow front that has already settled to the back side of the debris. Therefore, the macroviscous fluid settles (completely stops to flow) 20% faster than the grain-inertia fluid. Due to the dispersive pressure in grain-inertia fluid, the settlement process is delayed by 20% for the grain-inertia fluid than for the macroviscous fluid. This is meaningful because particles are more agitated due to higher dispersive pressure in grain-inertia fluids than in macroviscous fluids. Once the material comes close to rest, these dispersive forces (induced by the quadratic shear-rate), are still active for grain-inertia fluid but macroviscous fluid settles relatively faster because it is less dispersive. This provides a tool to approximate and estimate the final settlement time (the time at which the entire fluid body is at rest). So, Eq. (13) establishes a new scaling law for the settlement (the depositional process) of the Bagnold's fluids. Although this is intuitively clear, it must still be verified with experiments. This is not within the scope of this paper and is deferred to future work. Furthermore, the solutions for velocity show many interesting phenomena as they describe the process of deposition. The front ($x=0$) comes to rest (settlement) at first, and this information travels back-

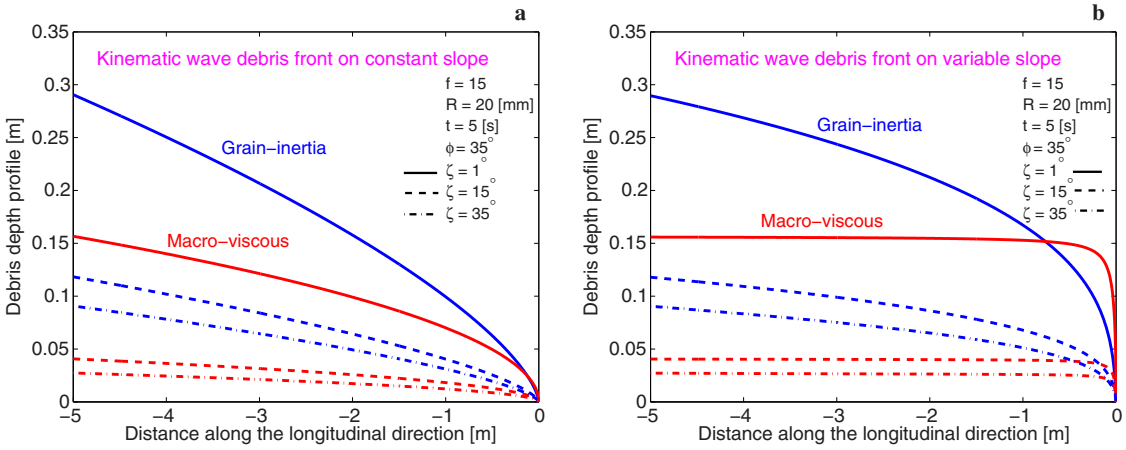

FIG. 1. (Color online) Effect of the slope angle on the debris flow front for fixed internal friction angle and three different slopes: (a) constant slope; (b) variable slopes in which the slope varies continuously from 1° (solid lines), 15° (dashed lines), and 35° (dot-dashed lines) for $-5 \le x$ to zero at the flow front ($x=0$) for all curves. Looking from the top left, the first two curves are for grain-inertia and macroviscous ($\zeta=1°$), next two curves are for grain-inertia and macroviscous ($\zeta=15°$), and the last two curves are for grain-inertia and macroviscous ($\zeta=35°$) deformation, respectively.

ward, linearly in space but inversely with time, until the tail comes to rest. For relatively large time ($t \to \infty$), the body is at rest everywhere (completely settled). One also observes such phenomena in the deposition in laboratory experiments or in natural events.[11,15,35,36]

E. Parameter studies

Here we analyze the influence of the parameters based on Λ (Λ_{gi} or Λ_{mv}) and solutions Eqs. (9) and (11). Since the parameters R, f (f_{gi} or f_{mv}), and ϕ are in the denominator and ζ is in the numerator of Λ, it would suffice to investigate the results with ϕ and ζ. Λ_{gi} and Λ_{mv} are the magnifying factors and the quality of the depth profiles depend on the exponents 2/3 or 1/2 applied to the similarity variable $-x/t$ for the grain-inertia and the macroviscous fluids, respectively. So, for ease of comparison, numerical values of f_{gi} and f_{mv} are set equal.

Figure 1(a) shows that, for constant slope angles, as slope decreases the flow depth increases both for grain-inertia and macroviscous fluids. Similar observations are also presented in Iverson and Denlinger.[13] This is due to the fact that as the slope increases, the material slides faster and it is more probable for longitudinal stretching and thus thinning the depth profiles. However, the front heights associated with the grain-inertia flows dominate the corresponding front heights of the macroviscous flows. This can be explained mechanically as follows: In the grain-inertia flows, the shear and normal stresses vary quadratically with the shear-rate, whereas this relation is linear for the macroviscous flows. Therefore, the dispersion of Bagnold's grain-inertia flow induces higher normal stress effects, which in turn is responsible for the higher depths of the flow fronts when compared to the macroviscous fluids. Note that although the depth-averaged form of the mass balance is used, the dispersive nature of the flow and the normal stress effect is retained in Λ_{gi} that emerges from Eq. (3). Figure 1(b) presents debris flow front geometry in which the slope is varied to drop from higher values to zero in the domain $-5 \le x \le 0$. Although the qualitative behavior of the flow front for the grain-inertia fluid has also been changed substantially, the front profiles for the macroviscous fluids are changed drastically. Very steep fronts are developed in the immediate vicinity of the front ($x=0$) like in the yield stress fluid (see Ancey[27]). However, for all slopes, immediately behind the front, the shape of the flow profile is nearly parallel to the sliding surface for the macroviscous flow. A further interesting point is that for both the grain-inertia and macroviscous flows, the fronts are bulging in the direction normal to the sliding surface. This is associated with the curvature of the bed. This is clear because as slope angle (ζ) decreases, Λ decreases and consequently the depth profile increases. This increase in the depth profile is higher as one moves close to the debris front. The rather interesting point is that such an increase in the depth is much more intensified for the macroviscous fluid than in the grain-inertia fluid. Another important observation is that the macroviscous flow profile begins to dominate the grain-inertia flow profile from the front of the flow. This is attributed to the curvature drop to zero at the flow front. The main reason for the dramatic change in the form of the front profile in the macroviscous fluid is that the depth profile is proportional to $(x/t)^{1/2}$, while in the grain-inertia flow the depth profile is proportional to $(x/t)^{2/3}$.

For the case of a mild slope channel (e.g., either constant (1°) or the slope drops to zero from 1° in the upstream), the results are analyzed for different internal friction angles since it is one of the major material parameters that influences the front of the flow and the depositions (see Pudasaini and Kröner[36]). A similar analysis could be performed for the particle diameter or the solid volume fraction. The internal friction angle is chosen to be 15°, 25°, and 35°. From a mechanical point of view, the material with higher internal friction angle produces higher dilation under applied shear load. This dilation is then responsible for creating the normal stress effect in the direction perpendicular to the flow and increasing the flow depth.

Since in the macroviscous fluid the normal and shear stresses are only linearly related to the shear-rate, the dilatational effect is nominal as compared to the same effect with

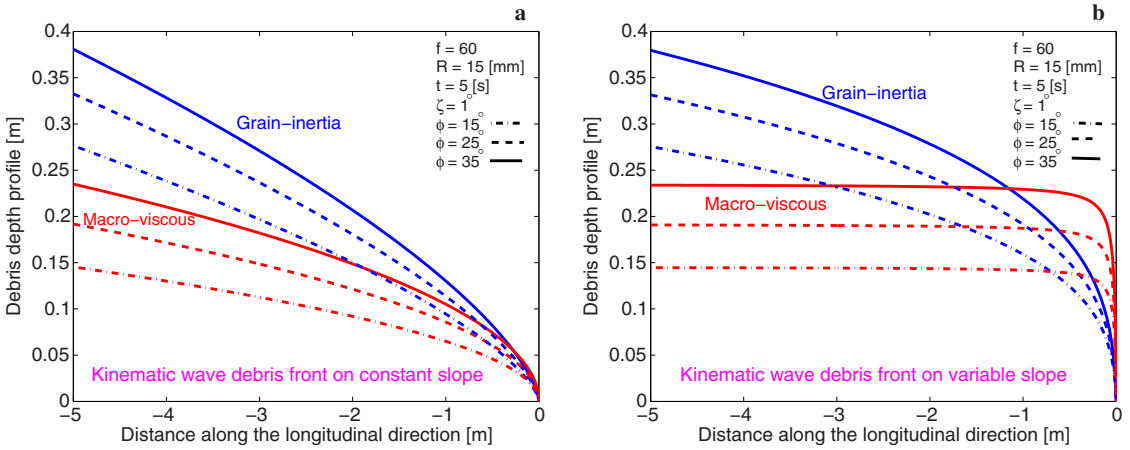

FIG. 2. (Color online) Effect of grain friction on the debris flow front for three different internal friction angles: (a) constant slope; (b) variable slope, which varies continuously from 1° to zero. Other notations are as in Fig. 1. Looking from the top left, the first three curves are for grain-inertia and the last three curves are for macroviscous deformation, respectively.

the grain-inertia flows where the shear and normal stresses are quadratically related to the shear-rate. This is clearly manifested in the plot [Fig. 2(a)] in which each curve (for different internal friction angles) for the grain-inertia flow profile dominates the corresponding curves in the macroviscous flows. Figure 2(b) presents results analogous to Fig. 1(b), where the bed curvature drops to zero at the flow front.

It is worth mentioning a few words on the front shape of the flow down the curved slope. The bed curvature produces a sharp front during the flow, which may then diffuse during the settlement (deposition) process. Such profiles are also observed when numerically solving the full kinematic Eq. (7). This results because including pressure gradient ($\varsigma \neq 0$, Fig. 4), or introducing the basal curvature [Figs. 1(b) and 2(b)], both induce rapid resistance in the front. The front is sharper for the macroviscous fluid than the grain-inertia fluid because of the higher material strength in the latter case. The higher strength resists bulging of the material. The situation in which the pressure gradient is not negligible is included in another type of exact solutions describing the fronts in Secs. II F and III. A further discussion on the effect of the pressure gradient on the front shape and the geometric profile of the flowing mass is presented in Sec. III C.

F. The wave phenomena

The kinematic wave Eq. (7a) is solved numerically by applying the shock capturing TVD-NOC numerical scheme with the Minmod limiter (see, e.g., Pudasaini and Hutter,[11] Nessyahu and Tadmor,[24] and Tai *et al.*[25]). The numerical solutions are presented in Fig. 3 for the triangular initial debris profile and $\varsigma=0$. The model parameters are set as $\Lambda_{gi}=0.2$ and $\Lambda_{mv}=0.31$. The mechanisms of the wave advection and distortion are described by the fluxes ($\mathcal{F}_{gi}$, $\mathcal{F}_{mv}$) and the wave speeds ($\mathcal{C}_{gi}$, $\mathcal{C}_{mv}$), respectively, for the grain-inertial and macroviscous fluids. The simulation results show that the depth profiles are continuously distorted as time elapses. Once the front fully transforms into a shock or a depth bore (perpendicular to the slope) at times $t^s_{gi}=2.8$ s for the grain-inertia and $t^s_{mv}=2.33$ s for the macroviscous fluids, the fronts propagate downstream (virtually) without changing the shape while stretching the body in the longitudinal direction. This is the underlying property of the hyperbolic wave equation applied to the shock capturing TVD-NOC scheme.[24] The quasiasymptotic behavior could be seen in the front structure of the time-dependent solution. However, generally, there is no asymptotic limit of the simulation. Furthermore, the macroviscous wave transforms into a perfect depth bore faster than the corresponding grain-inertial wave. The free-surface of the grain-inertia wave at t^s_{gi} is almost a straight line whereas the free-surface of the macroviscous wave is still

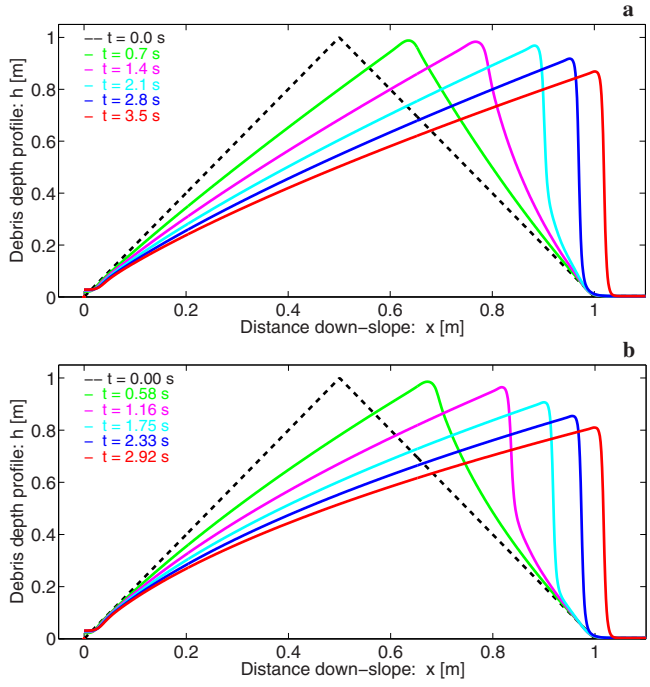

FIG. 3. (Color online) Distortion and propagation of the kinematic waves for the (a) grain-inertial and (b) macroviscous fluids as the motion starts from the initial triangular debris profile. Simulations are obtained by solving the nonlinear kinematic wave Eq. (7) by neglecting the hydraulic gradient.

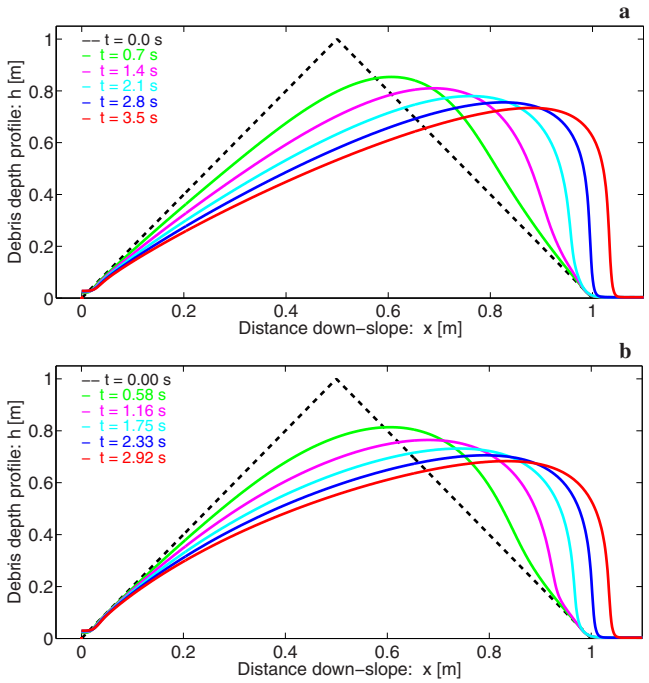

FIG. 4. (Color online) Distortion and propagation of the kinematic waves for the (a) grain-inertial and (b) macroviscous fluids as the motion starts from the initial triangular debris profile. Simulations are obtained by solving the nonlinear kinematic wave Eq. (7) by including the hydraulic gradient.

concave downward even at t^s_{mv}. This phenomenon is attributed to the fluxes and the wave celerities, corresponding to the two different material behaviors.

Next, we solve the full advection Eq. (7) with $\varsigma=0.25$ that includes the earth pressure coefficient and the free-surface pressure gradient. Figure 4 shows that the pressure gradient term smoothes out the sharp front, and the kink at the forehead of the free surface as seen in the wave simulations without the pressure gradient term in Fig. 3 both for the grain-inertial and the macroviscous fluids. Ultimately, for both fluids the waves develop into the sharp shock fronts. Such fronts are also observed in debris flows (see, e.g., Iverson,[12] Pudasaini *et al.*,[15] and Hungr[26]). Our preliminary observations indicate that one can produce them with ketchup, honey, concrete, or mud sliding down a ramp. However, such geometries are yet to be verified with suitable experiments. Furthermore, due to the associated pressure gradient dependent fluxes, the deformations of the debris bodies are different. The head of the macroviscous flow is more rounded as compared to the same with the grain-inertia fluid. Finally, note that from Eqs. (4) and (7) the associated velocity fields are also obtained.

A note on the pressure gradient and the front behavior is in order. We have analyzed both cases in Figs. 3 and 4, in which the pressure gradient is neglected and retained, respectively. We are not directly dealing with the momentum equation but the structure of the final Eq. (7a) is mainly controlled by the kinematic wave or the hyperbolic nature of the equation, which, due to its intrinsic behavior, could describe the sharp change of the field variables, e.g., the flow depth or the pressure gradient.

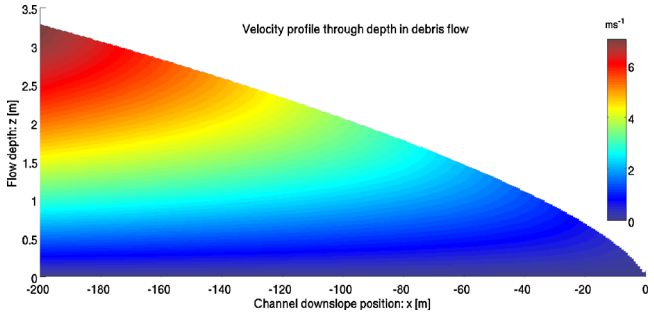

FIG. 5. (Color online) Reconstructed full two-dimensional plane velocity field of a debris flow through the depth and along the channel as described by Eq. (12).

G. Performance of the reconstructed velocity field through the flow depth

Figure 5 shows the reconstructed semiexact two-dimensional plane velocity field through the flow depth z and along the down-slope channel direction x for the debris flow head. In Fig. 5, the top surface is the free-surface of the flow. To this author's knowledge, such a general velocity field in exact solution form does not exist in the literature. The numerical values of the parameter are chosen as $t=19$ and $\Lambda_{gi}=1.76$, respectively. This figure shows that due to the dispersive dissipation in excess of the gravitational load in the longitudinal direction, the motion ceases (settlement or deposition process starts) from the front and the bottom simultaneously. This information then propagates backward and toward the top. Such behavior is important in sediment transport that deals with the depositional behavior of the material in the run-out zone. The upward concave curvature of the velocity field is also observed as one moves in the down-slope direction. Figure 6 shows the velocity distribution through the depth at different down-slope channel positions. These results are very similar to the results produced in molecular dynamics simulations by Silbert *et al.*[20] (Fig. 7). However, the advantage here is that we can work with the variable free-surface profile, the different down-slope positions, and time.

Figure 7 shows the direct mean velocity, from Eq. (9), and the mean velocity as obtained from the reconstructed velocity field Eq. (12) collapse completely. This demon-

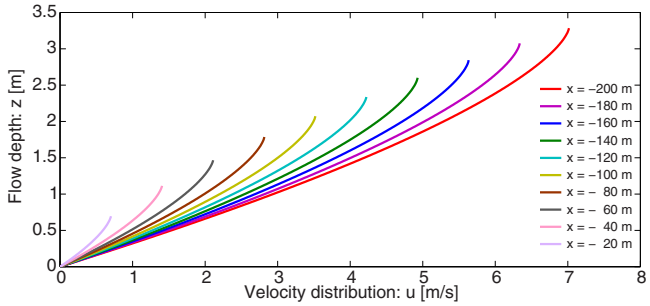

FIG. 6. (Color online) Velocity distribution through depth of a debris flow at different channel positions.

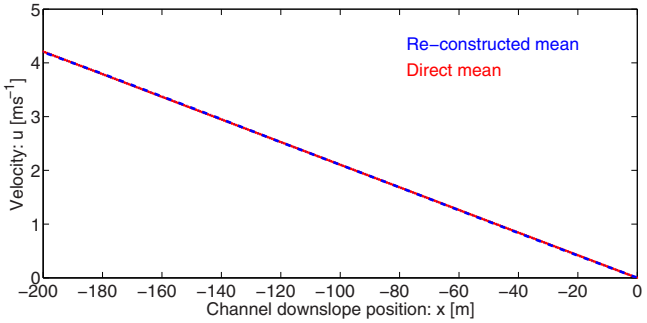

FIG. 7. (Color online) Mean from the reconstructed velocity field and direct mean velocity in a debris flow.

strates the consistency of our derivation and that the reconstructed depth variation of the velocity field is physically meaningful.

H. Comparison with experiment

Figure 8 shows a comparison between the theoretical prediction Eq. (12) and the experimental debris flow data from Takahashi.[6] For these results, the channel slope, particle diameter, and volumetric particle concentration are 20°, 0.005 m, and 0.31, respectively. As in Takahashi, the data and the predicted results are normalized with the surface velocity (u_{max}) and the flow depth h. There is a good comparison between the theoretical prediction and the experimental data. This adds confidence to the reconstructed velocity profiles through the depth and demonstrates its applicability in the debris flow events. Similar experimental data and numerical results are also presented in Takahashi.[5]

III. LAMBERT–EULER SOLUTION FOR DEBRIS FLOW FRONT

The debris flow front is modeled by using the Lambert–Euler omega function in mathematical physics. As in Sec. II, the flow takes place in an inclined channel. A shear-rate normal to the channel is assumed, but the pressure gradient is always retained. Note that usually pressure is neglected while simplifying the flow configuration in relation of the grain-inertia flows.[6,20,21] The motion is steady state (alternatively, the following equation is written in the reference frame moving with the front, or the shape of the front does not change in time: this is also an observed phenomenon, see, e.g., Pouliquen[34]) and satisfies Bagnold's grain-inertia (or macroviscous) motion. Therefore, the momentum balance takes the following form:

$$\rho g \cos\zeta h(\tan\zeta - \mathcal{P}K\,\partial h/\partial x) = \rho R^2 f(\nu)\tan\phi\gamma_b^2, \qquad (14)$$

where b indicates that the shear-rate ($\gamma=\partial\tilde{u}/\partial z$) is taken in the close vicinity of the basal surface (see, e.g., Pailha and Pouliquen[37]) and $\mathcal{P}$ is an empirical pressure gradient enhancement factor. The value of $\mathcal{P}$ will be constrained while calibrating the model equation with experimental or observed data; otherwise, it will be set equal to unity. $\mathcal{P}$ could also be introduced in Sec. II by incorporating it in ς, i.e., $\varsigma=\mathcal{P}K/\tan\zeta$ in Eq. (4). However, since in Sec. II exact solutions could be obtained in general only for negligible pressure gradient, it was not necessary to introduce $\mathcal{P}$ there. A detailed discussion on the mechanism and consequence of this factor will be presented later in Sec. III C. In order to develop the model equation, we set: $\mathcal{C}=-\mathcal{P}Kg\cos\zeta/[R^2f(\nu)\tan\phi\gamma_b^2]$, $\mathcal{D}=g\sin\zeta/[R^2f(\nu)\tan\phi\gamma_b^2]$, $H=\mathcal{D}h$, $\lambda=\mathcal{C}/\mathcal{D}^2$. We call $\mathcal{C}$ and $\mathcal{D}$ collective, and λ a unified model parameter. For a given debris flow, γ_b can effectively be assumed constant and lies in the range $1-100$ s^{-1}, see Ref. 12. Although λ may vary with the depth, in the close neighborhood of the basal surface, for a fully developed steady state flow it can assume a constant value with respect to the down-slope position, or at least local variation of λ with x being negligible (see, e.g., GDR MiDi[21] and Pouliquen[34]). Then, the force balance Eq. (14) takes a very special form of a nonlinear ordinary differential equation,

$$\lambda H\frac{dH}{dx} = 1 - H, \qquad (15)$$

with two singularities at $H=0$ and $\lambda=0$. Note that the singularity $\lambda=0$ is associated with the limiting cases, $\zeta=90°$ or $\partial\tilde{u}/\partial z=0$, which means either the material will leave the basal surface (free fall) or the shear-rate vanishes (gravity is balanced by the hydraulic gradient). In the latter case, the flow depth is uniform. This situation prevails in the backside of the front of the moving mass.[13,27,34,38,39] Exact solution for this equation can be constructed in a convenient explicit form,

$$H(x) = 1 + \mathcal{W}\left[(H_0-1)\exp\left((H_0-1)-\frac{x}{\lambda}\right)\right],\quad H_0 = H(x=0). \qquad (16)$$

In Eq. (16), $\mathcal{W}$ is the Lambert–Euler omega function,[40–44] which satisfies the special Lambert–Euler equation, $\mathcal{W}(x)e^{\mathcal{W}(x)}=x$.

For a steady state flow, one could also search for a solution in which the shear-rate $\gamma=u/h$ and the velocity of the

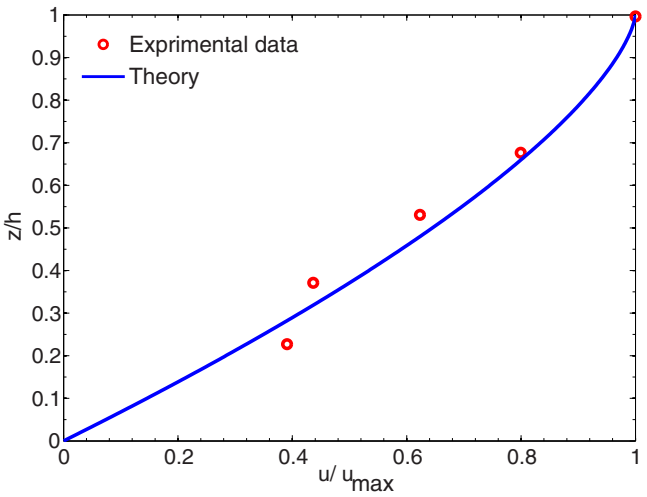

FIG. 8. (Color online) Comparison between theoretical prediction Eq. (12) and the experimental data from Takahashi [Ref. 6 (Fig. 2.28)] for the depth variation of the velocity field in a debris flow.

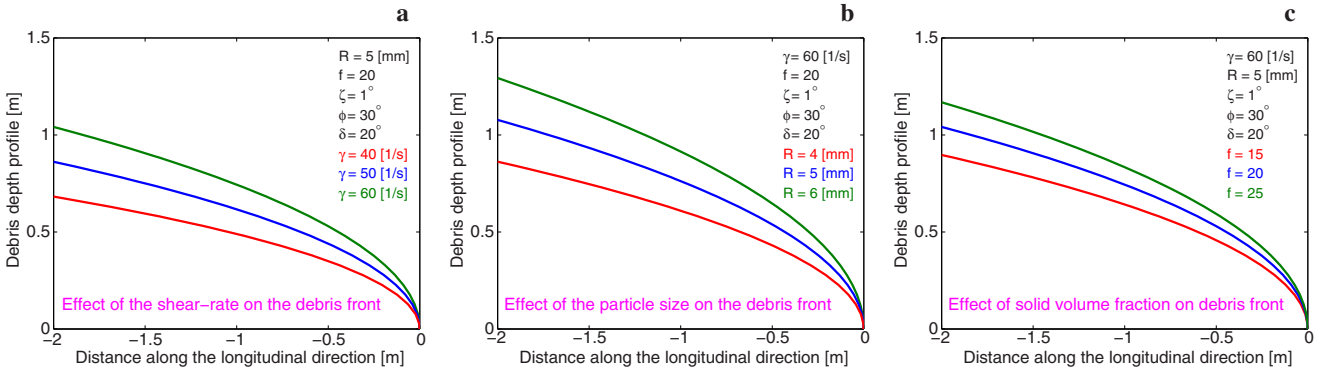

FIG. 9. (Color online) Influence of the shear-rate, particle size, and the solid volume fraction in the debris flow front.

propagating front is a constant (see Pouliquen[34]). Then the force balance Eq. (14) reduces to a nonlinear ordinary differential equation,

$$\frac{dh}{dx} = \frac{1 - \mathcal{D}h^3}{\mathcal{C}h^3}, \quad \mathcal{C} = -\frac{\mathcal{P}Kg\cos\zeta}{R^2 f(\nu)\tan\phi u^2}, \tag{17}$$

$$\mathcal{D} = \frac{g\sin\zeta}{R^2 f(\nu)\tan\phi u^2}.$$

With the initial condition $h_0 = h(x = x_0)$, the solution to this equation takes a bit complicated transcendental form ($\mathcal{D}^* = \mathcal{D}^{1/3}$),

$$x = x_0 + \frac{1}{6}\frac{\mathcal{C}}{\mathcal{D}^{*4}}\left[6\mathcal{D}^*(h_0 - h) + 2\sqrt{3}\arctan\left\{\frac{2\sqrt{3}\mathcal{D}^*(h - h_0)}{3 + (2\mathcal{D}^* h + 1)(2\mathcal{D}^* h_0 + 1)}\right\} + \ln\left\{\left(\frac{\mathcal{D}^{*2}h^2 + \mathcal{D}^* h + 1}{\mathcal{D}^{*2}h_0^2 + D^* h_0 + 1}\right)\left(\frac{\mathcal{D}^* h_0 - 1}{\mathcal{D}^* h - 1}\right)^2\right\}\right]. \tag{18}$$

Since Eq. (18) does not reproduce the data under consideration, we do not perform parameter study for this solution but compare with Eq. (16) and the experimental data in Sec. III B. However, Eq. (18) may still be applicable in other flow situations.

A. Influence of parameters

The physical parameters in model solution Eq. (16) consist of the particle size, solid volume fraction, bed friction angle, internal friction angle, the slope angle, and shear-rate at the sliding surface. Results show the effect of these parameters on the flow dynamics of the debris flow fronts. Figure 9 shows the influence of the shear-rate (a), particle size (b), and the solid volume fraction (c) in the debris flow front on mild slope. The (boundary) condition $h_0 = 0$ is set. Note that h_0 is an important parameter to fit the data (from experiments or observations) of debris flow front and depth profile. From a mechanical point of view, panel (a) is interesting as it shows that the debris flow height increases with increasing shear-rate. As explained earlier, this is related to the dilation induced by the higher quadratic shear-rate in the granular and debris mixture material under the applied shear load. This is a unique property of the granular and debris mixture in contrast to the usual fluid, which could not exhibit such effects.[11,45] It is worth quoting from Davies:[46] "… … as a mass thins by gravity, a given dilation may be maintained at successively lower values of $d\tilde{u}/dz$ [the shear-rate]." This explains the spreading of rock avalanche debris by mechanical fluidization. Similar to the shear-rate, the particle size, panel (b), and the solid volume fraction, panel (c), have positive influences on the dynamics of the height of the debris flow front. There is a simple reason for such effect; because the shear-rate, the particle size, and the solid volume fraction are (generally) all positively correlated with the dilation, which consequently amplifies the debris flow height.

Figure 10 shows the effect of the material friction, the internal (a) and bed friction (b) angles, and the slope angle of the channel (c). As in the case of the shear-rate, the internal friction angle has a positive influence on the debris flow height because higher internal friction angle can resist higher shear load. This finally leads to the higher dilation of the granular rich debris flows, which then increases the flow depth. On the contrary, the basal friction and the slope angle of the channel have negative influences on the depth of the debris flow front. Mechanically, it can be explained as follows: For smaller basal friction angle, the mass can slide easily with less deformation, but for higher basal friction angle, the mass is (relatively) held by the friction at the bed, and at the same time, gravity is effective in stretching and thinning the mass in the down-hill direction. The same is true for the higher slope angle. So, the slope and the basal friction angles both have positive effects in stretching the mass, thus reducing its flow height.[37]

The similarity solutions in Sec. II (and their plots in Figs. 1(a) and 2(a)) were computed by somehow including the shear-rate, the flow depth profile, and the time but neglecting the pressure gradient. Meanwhile, the Lambert–Euler solution presented in this section (Figs. 9 and 10) only considers the shear-rate at the sliding surface, and steady state flow is assumed but the effect of the earth pressure coefficient and the associated pressure gradient is included. Therefore, there are no direct and quantitative comparisons between these two types of solutions. However, these solutions can be compared qualitatively. Here we consider the

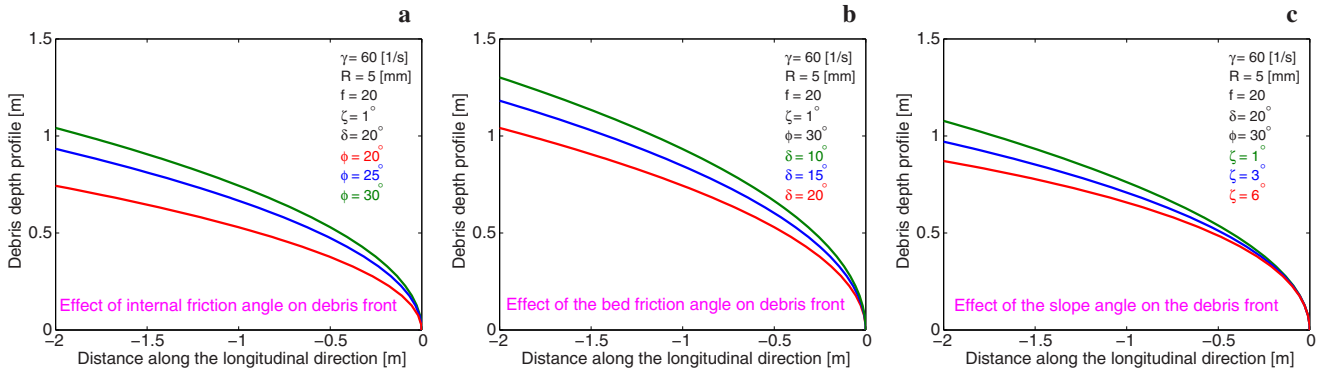

FIG. 10. (Color online) Influence of the internal and bed friction angles and the channel slope in the debris flow front.

case of the grain-inertia flows. The debris flow front described by the similarity solution is smooth and gentle [Figs. 1(a) and 2(a)] as compared to the flow front described by the Lambert–Euler equation (Figs. 9 and 10). The clifflike front head in the latter case is attributed to the pressure gradient. This is because mechanically, the sharp front head and the higher pressure gradient in the front represent the same phenomena, namely, a sharp change of the depth profile in that region. The most general solution is presented by Eq. (7) and is plotted in Fig. 4 as a high resolution shock capturing numerical simulation that includes all the physical properties of the flow under consideration. However, which of the solutions presented above describes the flow appropriately and to which extent depends on the flow situations. This may be an interesting and important direction for future research.

B. Comparison with observations

Granular and debris flow front and deposits, or the fronts of viscous fluids in natural events and in the laboratory experiments, can be described by solution Eq. (16). Comparing the two panels in Fig. 11, it is observed that the natural debris flow deposit can in principle be described by the grain-inertia solution.

A comparison between these predictions and the laboratory granular front propagation is presented in Fig. 12. The data are obtained from Pouliquen[34] describing the shape of granular front down a rough inclined plane. The physical parameters from the experiment are used to plot the model Eq. (16). The parameter values are: $\zeta=24.5°$, $R=0.0005$ m, $\nu=0.59$, the shear-rate$=71$ s^{-1}, and $f_{gi}=51$ (from Campbell[19]) for Eq. (16). The value of the pressure enhancement factor $\mathcal{P}$ is 3.5. With this, there is a good agreement between the model solution Eq. (16) and the experimental data. However, Eq. (18) is plotted with $u=0.2$ ms^{-1} (from Pouliquen) and $f_{gi}=51$ and two other very nonrealistic parameters, $R=0.0015$ m and $\mathcal{P}=28$, in order to approach the data, but otherwise it does not represent those data at all. This suggests that the steady state front propagation is better described with the constant shear-rate. Note that one cannot completely exclude the applicability of solution Eq. (18), which may find its place in flows other than those considered here.

For simplicity, the physical parameters are collectively grouped into $\mathcal{C}$ and $\mathcal{D}$, respectively. The exact solution, analogous to Eq. (16), can also be used to describe the wave front for a laminar dam break wave on inclined or horizontal channels. The results are presented in Fig. 13. Comparisons between our exact solutions with the experimental data using a glucose-syrup solution (see Debiane[38]), and the model predictions by Chanson,[39] are generally in very good agreement.

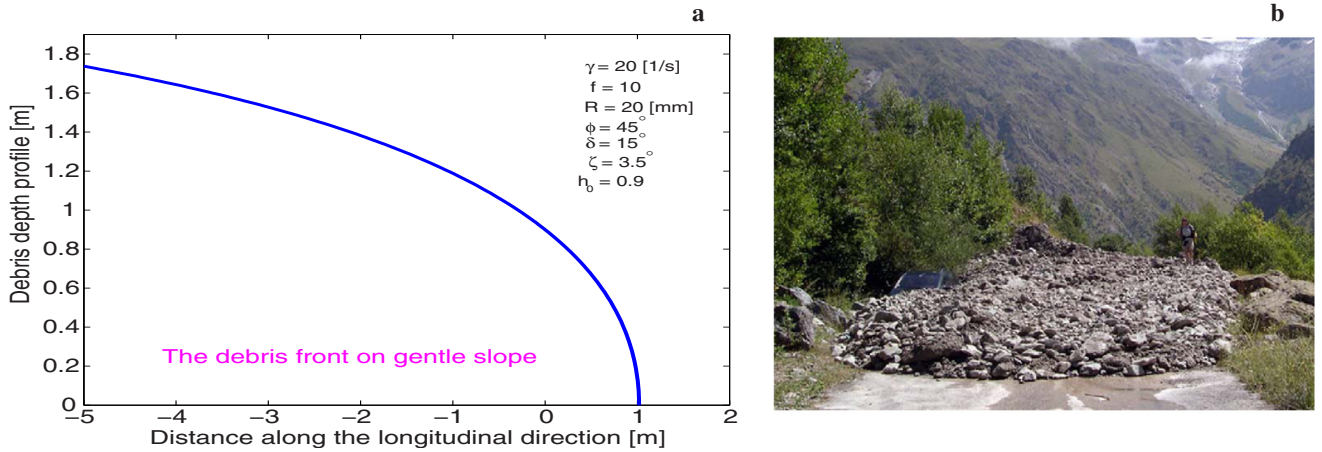

FIG. 11. (Color online) Debris flow deposit: (a) Results from present calculation. (b) Deposit lobe of a heavy rainfall induced debris flow in the Valgaudemar valley, France [from Ancey (Ref. 27)]. The deposit shape is similar to the left panel.

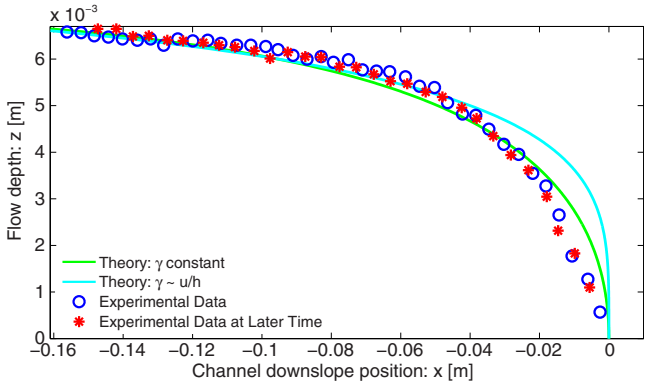

FIG. 12. (Color online) Granular front geometry on inclined rough plane, plotted with Eq. (16) and Eq. (18), respectively. Circles and stars are experimental data from Pouliquen [Ref. 34 (Fig. 1)]. Stars correspond to the front at 1.5 m downstream indicating that the flow is in steady state.

Note that Chanson used the diffusive wave equation to derive the wave tip solution for the dam break flows for the horizontal channel: $h=[-6\xi(c/\mathcal{R})x]^{1/3}$, $\mathcal{R}=\rho\sqrt{gh_0^3}/\mu$, where ξ is the flow resistance coefficient (a constant), μ is the dynamic viscosity, ρ is the density, h_0 is the initial flow height, $\mathcal{R}$ is the reservoir flow Reynolds number, c is the wave front celerity, and x is the coordinate along the channel measured from the wave tip to upstream. Similarly, the model solution derived by Chanson for the mild slope channel is

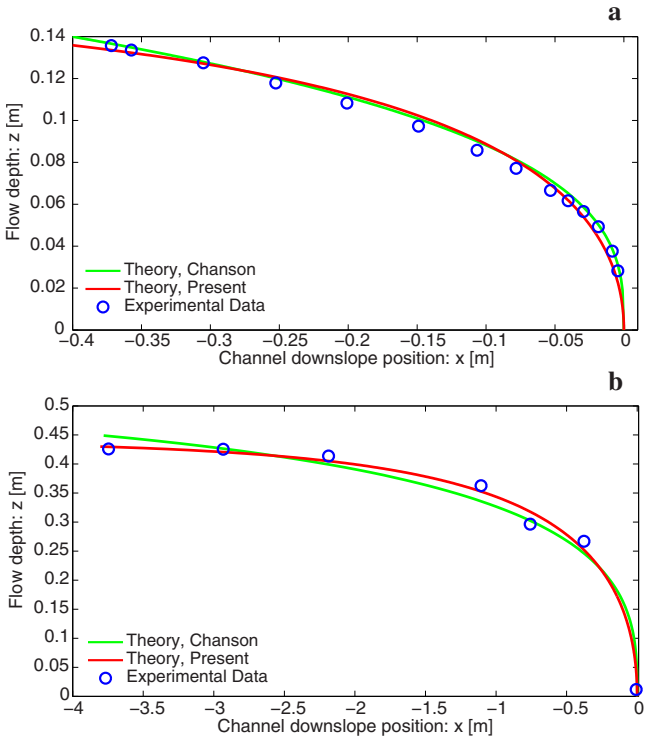

FIG. 13. (Color online) Wave front for a laminar dam break wave in (a) horizontal and (b) slightly inclined channel. Solid lines are results from present model solutions and Chanson theories (Ref. 39) for the macroviscous fluid. Circles are experimental data with glucose-syrup solution from Debiane (Ref. 38). The parameter values are: $(\mathcal{C},\mathcal{D})=(-15.53,\ 6.16)$ or $\lambda=-0.41$; $\xi=1, c=0.0064$, $\mathcal{R}=5.6$ for (a) and $(\mathcal{C},\mathcal{D})=(-7.01,\ 2.27)$ or $\lambda=-1.36$; $\xi u=0.000235$, $\mathcal{R}=0.77$, $\zeta=3°$ for (b), respectively.

$$x=-\frac{1}{\sin\zeta}\left[\sqrt{\frac{2\xi c}{\mathcal{R}\sin\zeta}}\operatorname{arctanh}\left(h\sqrt{\frac{\mathcal{R}\sin\zeta}{2\xi c}}\right)-h\right]. \tag{19}$$

C. The pressure gradient enhancement factor

Most, if not all, continuum mechanical models for mass flows are based on the assumption that the overburden pressure is hydrostatic.[12,14,28,31,32,47] However, in reality the pressure distribution in flowing granular and debris material is not hydrostatic in general. There have been some attempts to minimize this discrepancy by appropriately modeling the frictional term in the momentum (or the force) balance equation so as to obtain the required flow configuration. This can be achieved in two different ways.

(i) By differently modeling the basal frictional resistance by modifying the dry Coulomb friction, Pouliquen[33,34] pioneered a new empirical scaling law for the flow of granular material down a rough incline. In this law, the friction coefficient μ is expressed in terms of the mean velocity and the thickness of the granular layer. This includes two angles: θ_1, an angle where $h_{stop}(\theta)$ diverges, and θ_2, an angle where $h_{stop}(\theta)$ vanishes, where $h_{stop}(\theta)$ is the minimum thickness necessary to observe steady uniform flow at inclination θ. This model includes two further parameters, β, a fit parameter, and L, a characteristic dimensionless thickness over which $h_{stop}(\theta)$ varies. The expression for $h_{stop}(\theta)$ is derived from $\mu(u,h)=\tan\theta_1+(\tan\theta_2-\tan\theta_1)\exp[-\beta h/Ld(\sqrt{gh}/u)]$ and $u/\sqrt{gh}=\beta h/h_{stop}(\theta)$, where d is the particle diameter. Thus, θ_1, θ_2, and L are characteristics of material. This friction law, which has successfully been applied to granular flows, can adequately model the steady state front propagation.[21,33,34,48–50] However, there are some limitations. This law is mainly based on the smooth granular materials and the channel inclination is a slight perturbation from the internal friction of the granular material. The definition of μ makes it impossible to obtain an exact solution as in Eq. (16). In the limit as $\theta\to\theta_2$, the pressure gradient becomes zero and thus the flow profile is constant or uniform, which is not realistic, or at least very restricted and applies only to the far upstream of the sliding mass. Similarly, as $\theta\to\theta_1$ or $\theta_2\to\theta_1$, the front profile is indeterminate [see equation (5) in Pouliquen[34]]. These limitations are associated with the Coulomb law and the new definition of μ.

(ii) The above problems can, however, be overcome by employing Bagnold's grain-inertia law instead of using Coulomb friction to describe the granular and debris flows. And instead of modifying the frictional or the dissipation mechanism, we modify the hydraulic pressure gradient by empirically introducing a pressure gradient enhancing factor $\mathcal{P}$. In fact, either of them is responsible for introducing the appropriate stretching of the flow profile and controls the flow dynamics. The important point is that either modified friction or enhanced pressure gradient would ultimately control the down-slope gravitational load in such a way that the observed flow could be achieved. The single parameter $\mathcal{P}$ turned out to be very useful to fit the model solution Eq. (16) with experiments for different types of flows, as demon-

strated in Sec. III B. This is a new mechanism of the front dynamics of granular and debris flows. Although it requires detailed studies, there are some primary conjectures about the functional relationship of this parameter to other field quantities. As free-surface curvature $\mathcal{K}$ is one of the most potential candidates to generate nonhydrostatic pressure, $\mathcal{P}$ can principally be related to $\mathcal{K}$. One suggestion would be $\mathcal{P}=\mathcal{F}(\mathcal{K})$, e.g., $\mathcal{P}=\chi_1+\chi_2\mathcal{K}$, where $\chi_{1,2}$ are possibly two free parameters. Finally, it is pointed out that one should either keep hydrostatic pressure and use rate-dependent friction (Pouliquen), or use Bagnold's law and enhanced pressure gradient (the approach described here). Although both approaches lead to stretching and produce similar results, mechanically they have different origins. Nonzero free-surface gradient or the hydraulic gradient cannot be fully described by hydrostatic models. However, at present there exists no dynamic pressure model for granular and debris flows. So, we need some empirical models. We have presented one such simple model in the present paper.

IV. SOLUTIONS FOR RAPID GRANULAR FLOWS

In connection to the construction of the exact solutions, in the previous sections, mainly the front velocity and the front geometry of the granular and debris flow were considered. Here we address the nonlinear velocity field and depth profile for dry granular flows down the entire slope. The derivation of exact solutions for avalanche flows in steady state (in time) condition with Coulomb and grain-inertia laws will be considered. In recent years, there have been extensive studies on the temporal evolution of dam break flows of granular and debris materials.[39,51–55] In contrast, here we are interested in the steady state flows in which the material is discharged from the silo gate so that the volume flux remains constant over time.

A. Chebyshev radical solution

First, we utilize Mohr–Coulomb plasticity and solve the model equation exactly by using Chebyshev radicals. We consider the following frictional granular flow equations (see, e.g., Pudasaini and Hutter,[11,32] Savage and Hutter,[28] and Gray *et al.*[31]):

$$\frac{\partial h}{\partial t}+\frac{\partial (hu)}{\partial x}=0, \tag{20a}$$

$$\frac{\partial}{\partial t}(hu)+\frac{\partial}{\partial x}(hu^2)=g\Big\{(\sin\zeta-\tan\delta\cos\zeta)h-0.5\frac{\partial}{\partial x}(\mathcal{P}K\cos\zeta h^2)\Big\}. \tag{20b}$$

These are the depth-averaged mass and the momentum balance equations, respectively, for the flow of granular material down the channel of inclination angle ζ, in which t is the time, x is the length along the slope, h is the avalanche depth as measured normal to the sliding surface, u is the downslope velocity, g is the gravity constant, and $K=K(\phi,\delta)$ is the earth pressure coefficient as a function of the internal and bed friction angles, ϕ and δ, respectively. By assuming the steady state (see Pudasaini and Kröner[36] and Pudasaini and Domnik[56]), the mass balance reduces to a reciprocal relation between the flow depth and the velocity,

$$h(x)u(x)=h_0u_0, \tag{21}$$

where $h_0=h(x_0)>0$ and $u_0=u(x_0)>0$ at $x=x_0$ are the initial conditions. With Eq. (21), the momentum balance Eq. (20b) reduces to an exact differential for u

$$\frac{d}{dx}\left(\frac{u^2}{2}+\frac{\beta h_0u_0}{u}\right)=s,\quad s=g(\sin\zeta-\tan\delta\cos\zeta),\quad \beta=g\mathcal{P}K\cos\zeta, \tag{22}$$

where β is the collective overburden pressure (parameter). Here we deal only with accelerating flows, so $s>0$. This equation can be integrated with respect to x, and utilizing the initial condition $u=u_0$ (uniform initial u at, e.g., the silo gate), the solution for u can be written in cubic expression as follows:

$$u^3-(2sx-2sx_0+u_0^2+2\beta h_0)u+2\beta h_0u_0=0. \tag{23}$$

There exist exact solutions to Eq. (23), but in complicated algebraic form. Solutions can be constructed by using Chebyshev radicals. Consider the following Chebyshev equation:

$$u^3-3pu-q=0,\quad p=(2sx-2sx_0+u_0^2+2\beta h_0)/3,\quad q=-2\beta h_0u_0. \tag{24}$$

For convenience, we define $\mathcal{T}=q/p^{3/2}$. Since, $\mathcal{T}\in[-2,2]$ the following roots are obtained:

$$u_1=\sqrt{p}\mathcal{T}_{1/3}^{+},\quad u_2=-\sqrt{p}\mathcal{T}_{1/3}^{-},\quad u_3=-u_1-u_2;\quad \mathcal{T}_{1/3}^{\pm}=2\cos\left[\arccos\left(\pm\frac{\mathcal{T}}{2}\right)\Big/3\right]. \tag{25}$$

However, only $u=u_1$ is a feasible solution, which can be written in a complete form as follows:

$$u = 2\sqrt{\frac{1}{3}(2sx - 2sx_0 + u_0^2 + 2\beta h_0)}\,\cos\left[\arccos\left\{-\beta h_0 u_0\left(\frac{3}{2sx - 2sx_0 + u_0^2 + 2\beta h_0}\right)^{3/2}\right\} \Big/ 3\right]. \tag{26}$$

Therefore, Eqs. (21) and (26) constitute a closed and complete solution for the avalanche height and velocity profile for steady state flow of granular material down an inclined channel. Furthermore, Eqs. (21) and (23) can be combined together to have a second equation directly connecting the avalanche flow depth with the flow velocity:

$$u^2 + 2\beta h - 2sx - (u_0^2 + 2\beta h_0) + 2sx_0 = 0.$$

B. Grain-inertia

Second, we replace Coulomb stress by Bagnold's grain-inertia stress and assume the shear-rate at the immediate neighborhood of the sliding surface. Equation (22) takes the form of a separable ordinary differential equation,

$$\frac{du}{dx} = \frac{Au^2 - Bu^3}{u^3 - C}; \quad A = g\,\sin\,\zeta;$$
$$B = -R^2 f\,\tan\,\phi\gamma^2/h_0 u_0; \quad C = \mathcal{P}\beta h_0 u_0. \tag{27}$$

Equation (27) possesses an exact solution in transcendental expression, which, with the initial condition $u_0 = u(x = x_0)$, reads as follows:

$$x = x_0 + \ln\left\{\left[\left(\frac{A - Bu_0}{A - Bu}\right)^A \exp(B(u_0 - u))\right]^{1/B^2} \times\left[\left(\frac{u_0(A - Bu)}{u(A - Bu_0)}\right)^{B/A^2} \exp\left(\frac{u_0 - u}{Au_0 u}\right)\right]^C\right\}. \tag{28}$$

Third, we consider the grain-inertia fluid in which the shear-rate is proportional to u/h. In this case, Eq. (27) takes the form

$$\frac{du}{dx} = \frac{Au^2 - Bu^7}{u^3 - C}; \quad A = g\,\sin\,\zeta;$$
$$B = -R^2 f\,\tan\,\phi/(h_0 u_0)^3; \quad C = \mathcal{P}\beta h_0 u_0. \tag{29}$$

The exact solution to this equation takes a very complicated and lengthy transcendental form. Since the plot of Eq. (29) did not represent the flow under consideration, we do not write the solution here. However, Eq. (29) may still be useful to other flow situations, a subject of further investigation.

C. Model performance and comparisons with experimental data

In locations far downstream from the silo gate, the free-surface gradient of the rapid shear granular flow is much smaller when compared to that associated with the sharp front presented in Secs. II and III. However, pressure gradient plays an important role in the immediate vicinity of the silo gate. So, depending on the channel position, the value of $\mathcal{P}$ other than unity is also applicable. Figure 14 shows the profiles for the avalanche velocity described by the exact solution Eq. (26). The steady state flow velocity increases as the dry granular material rapidly flows down an inclined channel in which the material is continuously released from a silo gate placed at $x_0 = -1.9$ m. Note that there is a sudden increase in the velocity field just after the release of the material in the immediate down-slope vicinity of the gate. Afterwards, the velocity profile takes a smooth parabolic form, characteristic of the Coulomb rheology.

Experiments were performed in a 2.85 m long, 0.15 m wide rectangular Plexiglas channel inclined at $\zeta = 50°$. 30 L of PVC pellets (mean diameter 4 mm) were continuously released from the silo gate with an opening of 0.15 m. The internal and bed friction angles of the granular material are $\phi = 32°$ and $\delta = 20°$, respectively. To keep high resolution, measurements were made for the first 0.4 m length of the channel. Images were captured by using a high speed camera (Optronis, typically 1000 fps). The data were postprocessed with a particle image velocimetry algorithm to obtain the velocity field of the sliding particles when the flow became steady state. The data thus obtained for the velocity are compared with our model predictions, Eq. (26) for the Coulomb and Eq. (28) for grain-inertia flows (with parameters $f = 50$ and $\gamma = 26$ as observed in experiments) in Fig. 15. The agreement between the experiment and the theory for Coulomb material is good but the grain-inertia flow rheology significantly overestimates the flow velocity. The reason for this is the collisional and dispersive nature of Bagnold's grain-inertia flow in contrast to the Coulomb sliding law in which the particles are in close contact with the neighboring par-

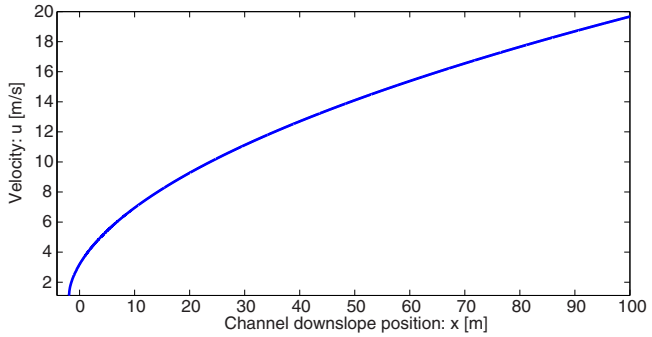

FIG. 14. (Color online) Theoretical prediction of the steady state velocity distribution in a rapid granular flow in an inclined channel. The flow is from left to right. Granular material is released continuously from the silo gate placed at $x = -1.9$ m. The parameters, $\zeta = 35°$, $\delta = 25°$, $\phi = 30°$, $u_0 = 1.1$ ms^{-1}, $h_0 = 0.2$ m, and $\mathcal{P} = 1$, respectively, are the channel slope, bed friction angle, internal friction angle, inlet velocity, inlet height, and the pressure gradient enhancement factor.

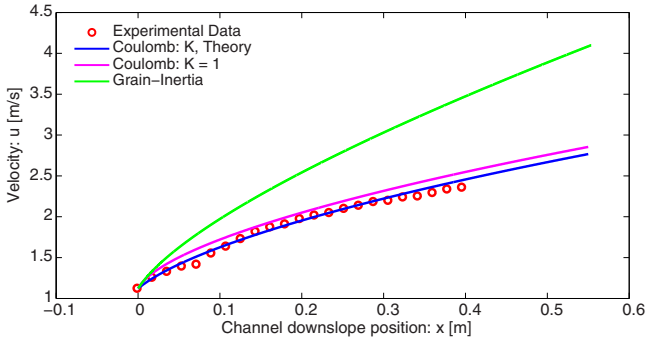

FIG. 15. (Color online) Comparison between the experimental and theoretical velocity distributions in rapid granular flow in an inclined channel for Coulomb and grain-inertia flows for $\mathcal{P}=1$. For Coulomb material, the effect of the material dependent ($K\neq 1$) or material independent ($K=1$) earth pressure coefficient is evident. The flow is from left to right. Granular material is released continuously from the silo gate placed at origin.

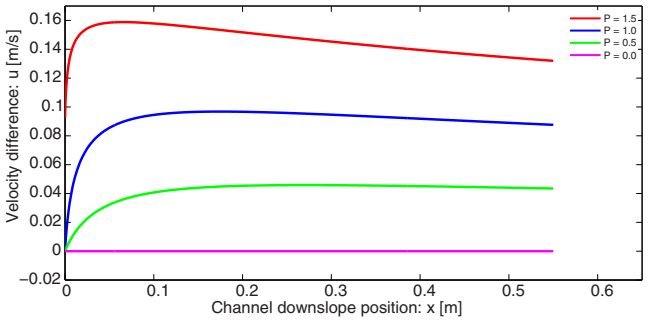

FIG. 16. (Color online) Difference in velocities when the earth pressure coefficient is $K=1$ and when it is computed from the theory as mentioned in Sec. IV A, in which case $K\neq 1$ for different values of the pressure gradient enhancement factor. $\mathcal{P}=1.0$ corresponds to solutions with Coulomb friction in Fig. 15.

ticles for which the dispersion is nominal. Thus, the simple Coulomb friction law can adequately describe the motion of rapid dense granular flows down the inclined channel.

D. Role of pressure gradient and viscous drag

There are effectively two model parameters in Eq. (26); the net driving acceleration s and the collective overburden pressure, $\beta=g\mathcal{P}K\cos\zeta$. In β, K is the earth pressure coefficient, a mechanical parameter and which depends on the internal and bed friction angles. This remains constant for extensional flows as considered in this section (see Pudasaini and Hutter[11]). When the flow is anisotropic (which is probably the case in most granular flows, at least at inception, during the flow obstacle interaction, and during the deposition), the value of K must be derived from soil mechanics theory. One such expression is mentioned in Sec. IV A for $K\neq 1$. For simplicity, if the granular flow is modeled as an isotopic material, $K=1$ is also used in simulations (see Pudasaini and Kröener[36] for a discussion on the effect of K). In Fig. 15, the exact solutions with Coulomb friction are plotted both for $K=1$ and $K\neq 1$. There are considerable differences between these two solutions and the data are better represented by the curve for which $K\neq 1$.

The parameter, $\mathcal{P}$, is the enhancement factor. The value of $\mathcal{P}$ may depend on the flow situation. In Fig. 15, these solutions are plotted for $\mathcal{P}=1$. The actual effect of $\mathcal{P}$ is observed in Fig. 16, in which the velocity difference between the solutions with $K=1$ and $K\neq 1$ are plotted for different values of $\mathcal{P}$. As expected, the difference increases rapidly just below the silo gate and tends to saturate far downstream. The difference decreases with the decreasing value of $\mathcal{P}$. However, the calculations show that the shape of the velocity difference curves depend on the value of the initial velocity and the value of $\mathcal{P}$. Therefore, K and $\mathcal{P}$ play important roles for appropriately modeling the pressure gradient in the flow.

It is worth mentioning that the rate-independent dry Coulomb friction law may not be able to adequately describe the flow of dry granular material when the channel length is very long and the area of interest is far downstream. In such a situation, the velocity may tend to saturate after some channel length. As discussed with the particle image velocimetry (PIV) laboratory data of the velocity field in Pudasaini and Hutter,[11] it is still an open question about how far downstream the dry Coulomb friction works. In principle, there can be two flow regimes: until some channel position $x\leq x_c$, dry Coulomb rheology is applicable; and when $x>x_c$, the regime changes to rate-dependent or viscous drag. In this situation, Pouliquen law[33,34] or Voellmy law[57] could be possible candidates to appropriately simulate the flow. However, due to the lack of adequate data and our inability to construct the exact solution analogous to Eq. (26) with variable friction or variable drag coefficient, we are unable to present further comparisons. Our next attempt would be to introduce the Voellmy drag $C_D u^2$ (see Pudasaini and Hutter,[11] Sec. 2.8.2) but in a Eulerian frame that also includes the pressure gradient $\partial h/\partial x$ as in the present analysis. However, note that the classical Voellmy solution is constructed with the assumption of a constant flow height, which results in "already after a very short starting distance almost the maximum velocity is reached … …," see Pudasaini and Hutter[11] and Voellmy.[57] Furthermore, experiments with relatively long (about 3 m) straight chutes with different inclination angles (between 30° to 45°) only weakly indicated the need for, but not strongly demanded for the introduction of, the drag force in rapid dry granular flows.[11] Therefore, experiments with much longer channels and with a much larger volume of granular materials are probably required to generate a definite answer to the question about the drag contribution. However, when the pressure gradient is included and we opt to cover both the near silo and far downstream flows, it may turn out to be very complicated to combine two solutions into a single mathematical structure.

V. SUMMARY

Three different types of exact solutions were presented for avalanching debris and granular flows down inclined slopes. Solutions are constructed for debris flows that obey Bagnold's rheology and for granular flows satisfying a dry Coulomb friction rheology. Solutions are derived both for time-dependent and steady state conditions for slow and rapid flows in the vicinity of the front and down the entire slope.

First, mass and noninertial momentum equations (with Bagnold's rheology) were combined to construct a very special kinematic wave equation in conservative form in which the flux and the wave celerity are complex nonlinear functions of the flow depth and the pressure gradient. For a particular choice of the flux, this equation takes the form of a nonlinear Burger equation. The full kinematic equation is solved for a triangular initial debris profile by implementing the TVD-NOC high resolution shock capturing numerical scheme. The simulation results demonstrate how the debris body advects down-slope after its release. Importantly, the pressure gradient and height dependent nonlinear flux and the wave celerity ultimately lead to the formation of shock structure in the moving front and stretching in the tail of the debris body. As observed in many debris flow events, such a typical geometric deformation of the debris mass and formation of the shock front are intrinsic properties of debris mass sliding and deforming down-slope. Furthermore, the pressure gradient smooths out the sharp front and the kink at the forehead of the free surface. The macroviscous wave transforms into a perfect depth bore faster than the corresponding grain-inertial wave. The head of the macroviscous flow is more rounded as compared to the head with the grain-inertia fluid. Based on the kinematic wave equation, exact solutions for the debris flow fronts and velocity profiles are constructed both for Bagnold's grain-inertia and macroviscous fluids. Important relationships are established concerning the settlement time and the settlement lengths between the grain-inertia and the macroviscous fluids, which show that the macroviscous fluid settles 20% faster than the grain-inertia fluid. Also, a new semiexact solution for the plane velocity profile through depth is constructed as an explicit function of the down-slope channel position, time, and the material as well as geometric parameters. From the solution, it is observed that, due to the dispersive dissipation in excess of the gravitational load, the motion ceases (deposition process starts) simultaneously from the front and the bottom. This information then propagates backward and toward the top.

The second types of exact solutions are constructed for the steady state debris flow front in which the force balance consists of Bagnold's grain-inertia or macroviscous forces, gravity, and the hydraulic pressure gradient, which is also accompanied by the pressure gradient enhancement factor. The exact solution is described in terms of the well known Lambert–Euler omega function. It is also demonstrated that measurement data of steady state front propagation of granular material are better described with some constant shear-rate at the base rather than the variable shear-rate. The pressure gradient enhancement factor is found to be crucial in properly controlling the stretching of the flow that largely assists calibration of the model solution with experimental data. This is a new mechanism of the front dynamics of granular and debris flows.

The third types of exact solutions are constructed for steady state rapid flows of granular material down the slope, where the flow is either governed by the Coulomb friction or by Bagnold's law. For Coulomb sliding, solutions are constructed in terms of Chebyshev radicals. The solution shows that the steady state flow velocity generally takes a parabolic form as the granular material rapidly flows down in which the material is continuously released from a source. By comparing the laboratory data of granular flow down an inclined channel, it is observed that the simple Coulomb sliding law with anisotropic earth pressure coefficient predicts the flow dynamics; just below the uniform release of the granular material from the silo; much better than the Bagnold's grain-inertia flow law.

Intensive parameter studies for all solutions are presented. The parameters include (i) the geometric parameters: the slope angle and its variation; and (ii) the physical parameters including the internal and bed friction angles of the debris, the particle diameter, the shear-rate, the solid volume fraction, the earth pressure coefficient, the pressure gradient enhancement factor, and the long-time behavior. The shear-rate, particle size, solid volume fraction, and the internal friction angle are all positively correlated with the dilation, which consequently amplifies the debris flow height. On the contrary, the basal friction and the slope angle of the channel have negative influences on the depth of the debris flow front.

In all cases, these simple exact solutions compare very well with field and laboratory data of granular or debris flows and flows of viscous fluids, their wave fronts, and deposits. This includes debris flow experiments, the motion of a glucose-syrup solution in the form of the laminar dam break waves in inclined or horizontal channels, laboratory granular front propagation, and stretching of granular material down rough and smooth inclined planes, both for slow and rapid motions. The present exact solutions and their analyses improve our understanding of mass flows, and can be used to calibrate numerical models. Therefore, these solutions can be of practical importance while describing the avalanches and debris flow dynamics and the dynamics of fronts and their deposits.

ACKNOWLEDGMENTS

We thank the German Science Foundation (DFG) for the financial support through the Project No. PU 386/1–1,2: Transition of a Granular Flow into the Deposit. We are grateful to Stephen A. Miller and Boris Galvan for fruitful discussions, and three anonymous referees for their constructive comments, which helped to improve the quality of the paper. Christian Kröner for experimental data of Fig. 15, and Vera Schmidt for digitizing the data are also greatly acknowledged.

[1] A. M. Johnson, *Physical Processes in Geology* (Freeman, San Francisco, 1970).
[2] A. Daido, "On the occurrence of mud-debris flow," Bull. Disas. Prev. Res. Inst.; Kyoto Univ., Japan **21**, 109 (1971).
[3] T. Takahashi, "Mechanical characteristics of debris flow," J. Hydr. Div. **104**, 1153 (1978).
[4] T. Takahashi, "The occurrence and flow mechanism of debris flow," Tsuchi to Kiso **26**, 45 (1978).
[5] T. Takahashi, "Debris flow," Annu. Rev. Fluid Mech. **13**, 57 (1981).
[6] T. Takahashi, *Debris Flow: Mechanics, Prediction and Countermeasures* (Taylor and Francis, Leiden, 2007).
[7] S. Egashira, K. Ashida, S. Tanonaka, and T. Takahashi, "Bed-load formula derived from constitutive equations of solid particle–water mixture," Bull. Disas. Prev. Res. Inst.; Kyoto Univ., Japan **34B**, 261 (1991).

[8]A. Armanini and P. Scotton, "Experimental analysis on dynamic impact of a debris flow on structure," Proceedings of the International Symposium INTERPRAEVENT 1992, Bern, 1992, Vol. 6.
[9]J. S. O'Brien, P. Y. Julien, and W. T. Fullerton, "Two-dimensional water flood and mudflow simulation," J. Hydraul. Eng. **119**, 244 (1993).
[10]P. Brufau, P. Garcia-Navarro, P. Ghilardi, L. Natale, and F. Savi, "1D mathematical modelling of debris flow," J. Hydraul. Res. **38**, 435 (2000).
[11]S. P. Pudasaini and K. Hutter, *Avalanche Dynamics: Dynamics of Rapid Flows of Dense Granular Avalanches* (Springer-Verlag, Berlin, 2007).
[12]R. M. Iverson, "The physics of debris flows," Rev. Geophys. **35**, 245, doi:10.1029/97RG00426 (1997).
[13]R. M. Iverson and R. P. Denlinger, "Flow of variably fluidized granular masses across three-dimensional terrain 1. Coulomb mixture theory," J. Geophys. Res. **106**, 537, doi:10.1029/2000JB900329 (2001).
[14]E. B. Pitman and L. Le, "A two-fluid model for avalanche and debris flows," Philos. Trans. R. Soc. London, Ser. A **363**, 1573 (2005).
[15]S. P. Pudasaini, Y. Wang, and K. Hutter, "Modelling debris flows down general channels," Nat. Hazards Earth Syst. Sci. **5**, 799 (2005).
[16]H. Hutter, B. Svendsen, and D. Rickenmann, "Debris flow modelling: A review," Continuum Mech. Thermodyn. **8**, 1 (1996).
[17]M. Arattano, L. Franzi, and L. Marchi, "Influence of rheology on debris flow simulation," Nat. Hazards Earth Syst. Sci. **6**, 519 (2006).
[18]R. A. Bagnold, "Experiments on a gravity-free dispersion of large solid spheres in a Newtonian fluid under shear," Proc. R. Soc. London, Ser. A **225**, 49 (1954).
[19]C. S. Campbell, "Rapid granular flows," Annu. Rev. Fluid Mech. **22**, 57 (1990).
[20]L. E. Silbert, D. Ertas, G. S. Grest, T. C. Halsey, D. Levine, and S. J. Plimpton, "Granular flow down an inclined plane: Bagnold scaling and rheology," Phys. Rev. E **64**, 051302 (2001).
[21]GDR MiDi, "On dense granular flows," Eur. Phys. J. E **14**, 341 (2004).
[22]M. L. Hunt, R. Zenit, C. S. Campbell, and C. E. Brennen, "Revisiting the 1954 suspension experiments of R. A. Bagnold," J. Fluid Mech. **452**, 1 (2002).
[23]R. W. Fox and A. McDonald, *Introduction to Fluid Mechanics*, 5th ed. (Wiley, New York, 2001).
[24]H. Nessyahu and E. Tadmor, "Non-oscillatory central differencing for hyperbolic conservation laws," J. Comput. Phys. **87**, 408 (1990).
[25]Y. C. Tai, S. Noelle, J. M. N. T. Gray, and K. Hutter, "Shock-capturing and front tracking methods for granular avalanches," J. Comput. Phys. **175**, 269 (2002).
[26]O. Hungr, "Analysis of debris flow surges using the theory of uniformly progressive flow," Earth Surf. Processes Landforms **25**, 483 (2000).
[27]C. Ancey, "Plasticity and geophysical flows: A review," J. Non-Newtonian Fluid Mech. **142**, 4 (2007).
[28]S. B. Savage and K. Hutter, "The motion of a finite mass of granular material down a rough incline," J. Fluid Mech. **199**, 177 (1989).
[29]C. Chen, "Comprehensive review of debris flow modeling concept in Japan," Rev. Eng. Geol. **7**, 13 (1987).
[30]C. Chen, "General solutions for viscoplastic debris flows," J. Hydraul. Eng. **114**, 237 (1988).
[31]J. M. N. T. Gray, M. Wieland, and K. Hutter, "Gravity-driven free surface flow of granular avalanches over complex basal topography," Proc. R. Soc. London, Ser. A **455**, 1841 (1999).
[32]S. P. Pudasaini and K. Hutter, "Rapid shear flows of dry granular masses down curved and twisted channels," J. Fluid Mech. **495**, 193 (2003).
[33]O. Pouliquen, "Scaling laws in granular flows down rough inclined planes," Phys. Fluids **11**, 542 (1999).
[34]O. Pouliquen, "On the shape of granular fronts down rough inclined planes," Phys. Fluids **11**, 1956 (1999).
[35]S. P. Pudasaini, S.-S. Hsiau, Y. Wang, and K. Hutter, "Velocity measurements in dry granular avalanches using particle image velocimetry technique and comparison with theoretical predictions," Phys. Fluids **17**, 093301 (2005).
[36]S. P. Pudasaini and C. Kröner, "Shock waves in rapid flows of dense granular materials: Theoretical predictions and experimental results," Phys. Rev. E **78**, 041308 (2008).
[37]M. Pailha and O. Pouliquen, "A two-phase flow description of the initiation of underwater granular avalanches," J. Fluid Mech. **633**, 115 (2009).
[38]K. Debiane, "Hydraulique des Ecoulements Laminaires Surface Libre dans une Canal pour des Milieux Visqueux ou Viscoplastiques: Régimes Uniformes, Graduellement Varié, et Rupture de Barrage," Ph.D. thesis, University of Grenoble I, Rheology Laboratory INPG-UJF-CNRS, France, 2000.
[39]H. Chanson, "A simple solution of the laminar dam break wave," J. Appl. Fluid Mech. **1**, 1 (2006).
[40]J. H. Lambert, "Observationes variae in mathesin puram," Acta Helvetica, physico-mathematico-anatomico-botanico-medica **3**, 128 (1758).
[41]J. H. Lambert, "Observations Analytiques," *Nouveaux Memoires de l'Academie Royale des Sciences et Belles-Lettres*, Vol. 1 (1770, 1772).
[42]L. Euler, "De serie Lambertina plurimisque eius insignibus proprietatibus," *Leonhardi Euleri Opera Omnia*, Ser. 1, Opera Mathematica (Birkhauser, Basel, 1992), Vol. 6, p. 350.
[43]D. A. Barry, J.-Y. Parlange, M. Sivapalan, and G. Sander, "A class of exact solutions for Richards equation," J. Hydrol. **142**, 29 (1993).
[44]R. M. Corless, G. H. Gonnet, D. E. G. Hare, D. J. Jeffrey, and D. E. Knuth, "On the Lambert W Function," Adv. Comput. Math. **5**, 329 (1996).
[45]O. Reynolds, "On the dilatancy of media composed of rigid particles in contact," Phil. Mag. Ser. **5**, 469 (1885).
[46]T. R. H. Davies, "Spreading of rock avalanches by mechanical fluidization," Rock Mech. **15**, 9 (1982).
[47]O. Hungr, "A model for the runout analysis of rapid flow slides, debris flows and avalanches," Can. Geotech. J. **32**, 610 (1995).
[48]O. Pouliquen and Y. Forterre, "Friction law for dense granular flows: Application to the motion of a mass down a rough inclined plane," J. Fluid Mech. **453**, 133 (2002).
[49]P. Jop, Y. Forterre, and O. Pouliquen, "A constitutive law for dense granular flows," Nature (London) **441**, 727 (2006).
[50]P. Jop, Y. Forterre, and O. Pouliquen, "Initiation of granular surface flows in a narrow channel," Phys. Fluids **19**, 088102 (2007).
[51]N. J. Balmforth and R. R. Kerswell, "Granular collapse in two dimensions," J. Fluid Mech. **538**, 399 (2005).
[52]E. Lajeunesse, J. B. Monnier, and G. M. Homsy, "Granular slumping on a horizontal surface," Phys. Fluids **17**, 103302 (2005).
[53]A. Mangeney-Castelnau, F. Bouchut, J. P. Vilotte, E. Lajeunesse, A. Aubertin, and M. Pirulli, "On the use of Saint-Venant equations to simulate the spreading of a granular mass," J. Geophys. Res. **110**, B09103, doi:10.1029/2004JB003161 (2005).
[54]A. J. Hogg, "Two-dimensional granular slumps down slopes," Phys. Fluids **19**, 093301 (2007) .
[55]C. Ancey, R. M. Iverson, M. Rentschler, and R. P. Denlinger, "An exact solution for ideal dam-break floods on steep slopes," Water Resour. Res. **44**, W01430 (2008).
[56]S. P. Pudasaini and B. Domnik, "Energy consideration in accelerating rapid shear granular flows," Nonlinear Processes Geophys. **16**, 399 (2009).
[57]A. Voellmy, "Über die Zerstörungskraft von Lawinen," Schweizerische Bauzeitung **73**, 159 (1955).